Multimode Decoupling Technique with Independent Tuning Characteristic for Mobile Terminals

Hang Xu, Hai Zhou, Steven Gao, Hanyang Wang, and Yujian Cheng

***Abstract*—The isolation between antenna elements is a key metric in some promising 5G technologies such as beamforming and in-band full-duplex (IBFD). However, multimode decoupling technology remains a great challenge especially for mobile terminals. One difficulty in achieving multi decoupling modes is that the operating modes of closely-packed decoupling elements have very strong mutual effect, which makes the tuning complicated and even unfeasible. Thus, in physical principle, a novel idea of achieving the stability of the boundary conditions of decoupling elements is proposed to solve the mutual effect problem; in physical structure, a metal boundary is adopted to realize the stability. One distinguished feature of the proposed technique is that the independent tuning characteristic can be maintained even if the number of decoupling elements increases. Therefore, wideband/multiband high isolation can be achieved by using multi decoupling elements. To validate the concept, two case studies are given. In a quad-mode decoupling design, the isolation is enhanced from 12.7 dB to > 21 dB within 22.0% bandwidth by using a $0.295\lambda_0 \times 0.059\lambda_0 \times 0.007\lambda_0$ decoupling structure. The mechanism of decoupling technique and the mutual effect between decoupling elements are investigated.**

***Index Terms*—Multimode decoupling elements, wideband decoupling, mutual coupling, 5G communication.**

I. Introduction

THE next generation of mobile wireless technology, i.e. 5th generation wireless systems (5G), will be able to deliver multi-gigabit-per-second data and efficiently support a much larger and more diverse set of devices than 4th generation wireless systems (4G) [1]. Beamforming and in-band full-duplex (IBFD) are very promising technologies for 5G [1-3]. One common feature of these technologies is the requirement of high isolation between antenna elements, because the strong mutual coupling among antenna elements will cause blind spot in wide-angle beam scanning array (beamforming) and severe self-interference (the major problem in an IBFD system) [3-5]. However, it is a great challenge to achieve good isolation in mobile terminals due to the limited space. Scientists have spent a lot of efforts on this problem.

Recently, some isolation enhancement methods have been reported including defected ground structure (DGS) [6], orthogonal polarization [7], characteristic mode [8], decoupling network [9], neutralization line [10], and decoupling element [11]. However, multimode decoupling technology remains a great challenge in compact application scenarios. DGS is bulky for mobile terminals such as smart phones [12-15]. A compact antenna array with orthogonal polarization is proposed for smart phones; acceptable isolations and good system performance are obtained [16]. Characteristic mode can achieve good isolation below 1 GHz [8], but it is difficult to manipulate the frequency of multi characteristic modes, because the freedom of modifying the radiator, i.e. the chassis, is very limited. Most decoupling networks are filter-like structures [17-20], so multi decoupling modes can be realized by referring to the design theory of multimode filter. Nevertheless, if the number of the decoupling modes rises, the design difficulty may become unacceptable due to the increased complexity of the corresponding matrix. [21] shows a design of three neutralization lines, but the layout is not flexible because the design needs to connect to specific locations of the antenna elements, and the neutralization lines affect each other.

To some extent, decoupling element can be identified as a wireless decoupling technology, so multi decoupling modes can be achieved by conveniently arranging a multimode decoupling element or multi single-mode decoupling elements between antenna elements or anywhere available. In [22], a tree-like multimode decoupling element was reported and achieved wideband isolation, but it is still bulky and does not show an easy-tuning feature; in theory, a miniaturized multimode resonator (decoupling element) is difficult to tune because of extremely complicated electromagnetic (EM) environment. Then another choice is to use multi single-mode decoupling elements, but the strong mutual effect between closely-packed decoupling elements is a large problem (it will be explained in Section II-B).

In this paper, a novel idea of achieving the stability of the boundary conditions of decoupling elements is proposed to solve the problem of strong mutual effect; a metal boundary is adopted to realize the stability by using its total-reflection feature. Benefiting from the achieved stability of the boundary

This work is funded by Huawei Technologies Ltd, China.

H. Xu and S. Gao are with the School of Engineering and Digital Arts, University of Kent, Canterbury, CT2 7NT, United Kingdom (e-mail: Hx21@kent.ac.uk and S.Gao@kent.ac.uk).

H. Zhou and H.Y. Wang are with Huawei Technologies Ltd, 300 South Oak Way, Green Park, Reading RG2 6UF, Berkshire, United Kingdom (e-mail: Hanyang.Wang@huawei.com and Hai.Zhou1@huawei.com).

Y.J. Cheng is with the EHF Key Laboratory of Fundamental Science, School of Electronic Engineering, University of Electronic Science and Technology of China (UESTC), Chengdu 611731, China (e-mail: chengyujian@uestc.edu.cn)

conditions, the operating modes of different decoupling elements can achieve independent tuning even if the edge-to-edge distance between these decoupling elements is only 3 mm ($0.035\lambda_0$ at 3.5 GHz and $0.024\lambda_0$ at 2.45 GHz). Besides, there is no limit for the number of the decoupling elements in this technique; in other words, *N*-1 metal boundaries can be inserted between *N* decoupling elements (*N* = 2, 3, 4, …). A distinguished feature of the proposed technique is that the independent tuning characteristic can still be maintained in the case of more decoupling elements (the key of the arrangement will be explained in Section III-B). As a result, wideband/multiband high isolation can be achieved by using multi decoupling elements. Two case studies are given to validate the concept. In a quad-mode decoupling design, the isolation is enhanced from 12.7 dB to > 21 dB within 22.0% bandwidth by using a $0.295\lambda_0 \times 0.059\lambda_0 \times 0.007\lambda_0$ decoupling structure. The mechanism of decoupling technique and the mutual effect between decoupling elements are investigated.

II. Methodology of Decoupling Elements Isolation Technique

In Section II-A, the configuration of an antenna array is introduced as the research scene. The mutual effect between decoupling elements is investigated and analyzed in Section II-B. In Section II-C, a novel physical idea and the corresponding physical structure are proposed to solve the mutual effect problem. The proposed idea is demonstrated in Section II-D. In Section II-E, some discussion is given.

A. Configuration Specification

A smart phone side-edge antenna array is shown in Fig. 1. There are three PCBs including Sub 1, Sub 2, and Sub 3. All the PCBs are 0.8 mm thick and double-sided FR4 (ε_r = 4.4, loss tangent = 0.02). The dimension of Sub 1 is $150 \times 75 \times 0.8$ mm^3 with 134×75 mm^2 metal ground on the bottom layer and 50 Ω microstrip lines on the top layer. There are two 75×8 mm^2 clearance areas. Sub 2 and Sub 3 ($134 \times 6.2 \times 0.8$ mm^3 for each) are perpendicularly placed on the top of Sub 1. Hence, the whole dimension of the antenna array is $150 \times 75 \times 7$ mm^3. The antenna elements including their feeding lines are symmetrically arranged along the two long edges of Sub 1.

The antenna elements in this paper are grounding strips, coupled-fed by coupling lines [23]**.** The grounding strips on Sub 2 and Sub 3 are grounded to the metal ground on Sub 1 through grounding points, and the coupling lines on Sub 2 and Sub 3 are connected to the 50 Ω microstrip lines on Sub 1 at connection points. In Fig. 1(b), the grounding strips are on the top layer of Sub 2 and the coupling lines are on the bottom layer. All the decoupling structures (not shown in Fig. 1) in this paper are on the same layer as the grounding strips. The antenna array in Fig. 1 is for explaining the configuration, and the detailed dimensions will be given in each example.

B. Mathematical and Physical Analysis of Mutual Effect between Decoupling Elements

In order to explain the problem of mutual effect, two decoupling elements, i.e. strip 1 and strip 2, are arranged between two antenna elements operating at 3.5 GHz in Fig. 2(a). The distance between Strip 1 and Strip 2 is only 3 mm. The decoupling elements in this paper are grounding strips without feeding lines. Because there are only 50 Ω microstrip lines and metal ground on Sub 1, only the structures on Sub 2 are shown for simplicity. The simulated S21 between Ant 1 and Ant 2 is shown in Fig. 2(b) and (c). To improve the isolation bandwidth, the resonant frequency of Strip 1 and Strip 2 needs to be tuned together. However, from the results in Fig. 2(b), when the resonant frequency of Strip 1 decreases from 4.045 GHz to 3.925 GHz (0.12 GHz), the resonant frequency of Strip 2 declines from 3.470 GHz to 3.370 GHz (0.1 GHz) as well. As a result, it is difficult to achieve wider isolation bandwidth by arranging the resonant frequency of two decoupling elements together. In such a small distance ($0.035\lambda_0$ at 3.5 GHz), the strong mutual effect seems unsolvable. To the author's knowledge, how to reduce the mutual effect between decoupling elements is still a blank field.

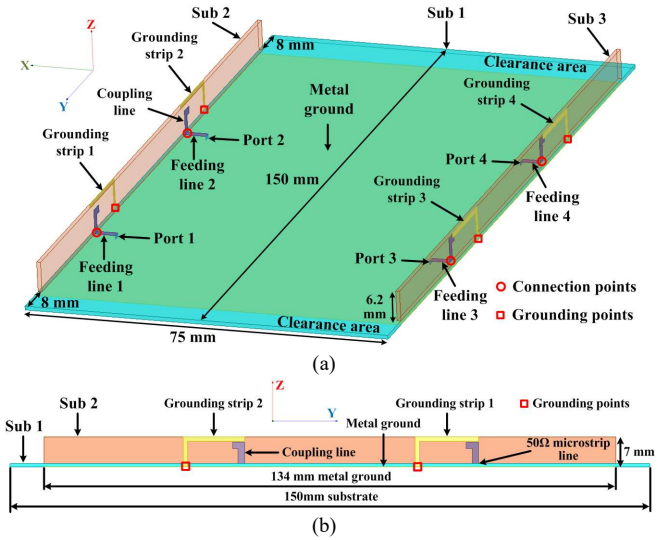

Fig. 1. Configuration of an antenna array. (a) Overall view. (b) Side view.

In this section, the investigation is on the basis of the solution property of Maxwell's equations [24]. In a solution region, the solution should contain all the EM information including the electrical characteristics of resonators. Obviously, resonant frequency of resonators is one of the electrical characteristics. Thus, the essence of the resonant frequency variation of the decoupling elements is that the solution of Maxwell's equations has changed in the corresponding solution region. Based on this analysis, there are three steps for the research: firstly, figure out in which solution region the solution can represent the main electrical characteristics of a decoupling element (Section II-B-1); secondly, in the chosen solution region, investigate the reason of the solution change (Section II-B-2); Lastly, propose some ideas to keep the solution stable (Section II-C).

1) Where Is Solution Region

An assumption will be used here: if in a solution region, the solution can represent the electrical characteristics of a decoupling element, most EM energy of the operating mode(s) of the decoupling element should distribute in that solution region. The decoupling elements used here are microstrip

resonators that operate at standing-wave modes. Standing-wave means that the EM field seems to stand on the metal track of a decoupling element itself without spreading, so the majority of the EM energy concentrates in the vicinity region of the decoupling element. The next paragraph is a demonstration for this conjecture.

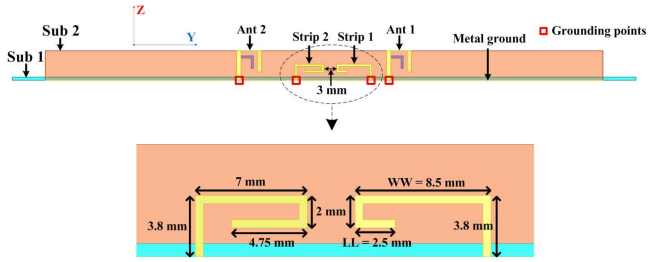

(a)

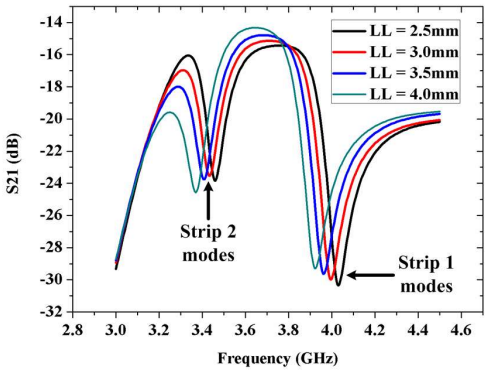

(b)

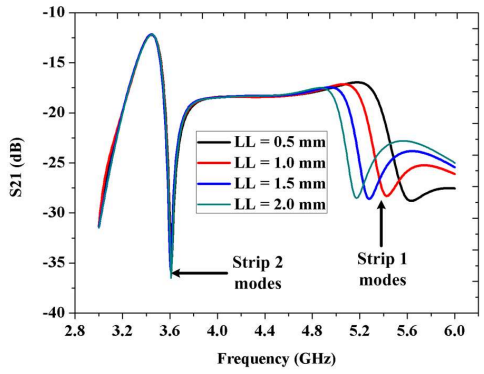

(c)

Fig. 2. An example for mutual effect. (a) Configuration. (b) S21 when WW = 8.5 mm. (c) S21 when WW = 5 mm.

All the discussion in this paragraph processes at the resonant frequency of Strip 2. Let us assume that the EM energy of Strip 2 distributes in a wide region, so there should be strong EM energy from Strip 2 distributing in the region of Strip 1 due to the very small distance (3 mm). Thus, even if the resonant frequency of Strip 1 is far from that of Strip 2 (this means that the energy from Strip 1 is very weak at the resonant frequency of Strip 2), the metal dimension change of Strip 1 should still have strong influence on Strip 2 because metal can greatly affect the EM field distribution. However, in Fig. 2(c), it can be seen that Strip 1 has little influence on Strip 2 when their resonant frequency is far from each other. The same phenomenon can be observed when Strip 1 is located on the left side of Strip 2. Therefore, even in the region very close to Strip 2, the EM energy from Strip 2 is still weak or null. Hence, the EM energy of Strip 2 should concentrate around itself instead of a wide distribution. The conclusion is the same for Strip 1.

Since the majority of the EM energy concentrates around a decoupling element itself, the solution in the vicinity region of the decoupling element should be able to represent its main electrical characteristics. For the ease of description, abstract models are extracted for Strip 1 and Strip 2 from Fig. 2(a) and shown in Fig. 3. Area A is the solution region of Strip 1, and Area B is the solution region of Strip 2.The solution in Area A and Area B can represent the main electrical characteristics of Strip 1 and Strip 2 respectively.

2) Why Does Solution Change

In order to investigate the reason of the solution change for Strip 2, a comparison between two situations is carried out: the first situation is that the resonant frequency of Strip 1 is far from that of Strip 2; the second situation is that the resonant frequency of Strip 1 is near that of Strip 2. The discussion in next paragraph processes still at the resonant frequency of Strip 2 and on the base of the models in Fig. 3.

According to the uniqueness theorem [24], in a fixed solution region, the solution can only be changed by varying the source and/or boundary conditions. However, in the solution region of Strip 2, i.e. Area B, there is no source. Therefore, the solution in Area B can only be altered by changing the boundary conditions. In the first situation, Strip 1 does not resonate, so the EM energy from Strip 1 is very weak on the boundary of Area B as shown in Fig. 3(a). When the resonant frequency of Strip 1 changes (still far from that of Strip 2), the EM energy from Strip 1 also changes on the boundary of Area B. Nevertheless, because the EM energy from Strip 1 is too weak compared to the energy of Strip 2, the energy fluctuation from Strip 1 cannot disturb the boundary conditions of Area B. As a result, the solution in Area B does not change, and thus the resonant frequency of Strip 2 remains the same. The results in Fig. 2(c) support the above analysis. In the second situation, the EM energy from Strip 1 is relatively strong on the boundary of Area B, which is shown in Fig. 3(b). When the resonant frequency of Strip1 changes (still near that of Strip 2), the EM energy from Strip 1 also changes on the boundary of Area B. Because the EM energy from Strip 1 is comparable to the energy of Strip 2 in this case, the energy fluctuation from Strip 1 disturbs the boundary conditions of Area B. As a result, the solution in Area B changes, and hence the resonant frequency of Strip 2 varies. The results in Fig. 2(b) also support the above analysis well.

Therefore, the mutual effect between decoupling elements should not be caused by the metal dimension change because the metal track of one decoupling element is out of the solution region of other decoupling elements in general. From the analysis in last paragraph, the essence of the mutual effect between decoupling elements is that the resonant frequency variation of one decoupling element leads to disturbing the

boundary conditions of the adjacent decoupling elements, so the solutions of Maxwell's equations vary in the corresponding solution regions. The solution change means the resonant frequency deviation of the adjacent decoupling elements.

C. Mechanism of Decoupling Elements Isolation Technique

Since the reason of the solution change is that the boundary conditions are disturbed, the key is to achieve the stability of the boundary conditions. Basically, there should be two kinds of thoughts including active methods and passive methods. The active methods are to initiatively compensate the EM field fluctuation on the boundary; for instance, similar to signal compensation technology, another excitation source might be introduced to provide an anti-fluctuation, but it would increase the complexity and the cost, and it should be difficult to provide accurate compensation in such complicated EM coupling environment. The passive methods are to block the EM energy from the adjacent regions through absorption or reflection: absorption methods seem unfeasible because it is difficult to find such small absorption material (< $7\times3\times0.8$ mm^3, i.e. $0.082\lambda_0\times0.035\lambda_0\times0.009\lambda_0$ at 3.5 GHz); therefore, reflection methods should be the proper choice. For reflection methods, there are also two different ways: one is to use different dielectrics with the permittivity of great difference so the EM field should reflect on the interface; the other is to use metal boundary which can be simply printed with PCB technology. Apparently, the first reflection method is more difficult to realize and its reflection effect should not be better than using metal boundary because metal boundary means total reflection. As a result, metal boundary is adopted in this paper.

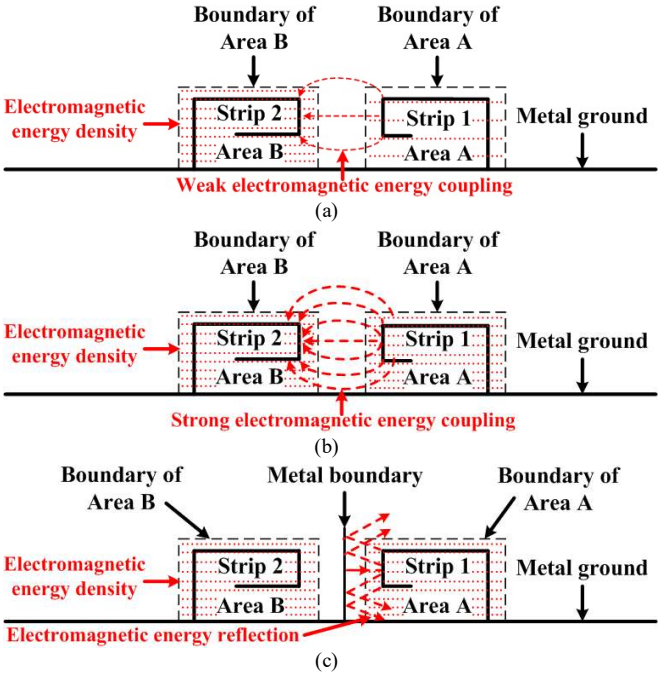

Fig. 3. Investigation model of mutual effect. (a) Weak coupling and (b) strong coupling without metal boundary. (c) Reflection effect of metal boundary.

To explain how a metal boundary can achieve the stability of the boundary conditions explicitly, an abstract model with a medal boundary between Strip 1 and Strip 2 is shown in Fig. 3(c); the metal boundary is connected to the metal ground. The discussion processes at the resonant frequency of Strip 2. When the resonant frequency of Strip 1 is near that of Strip 2, the EM energy from Strip 1 is relatively strong in Area A but very weak in Area B, because the metal boundary can reflect the majority of the EM energy as can be seen in Fig. 3(c). When the resonant frequency of Strip 1 changes (still near that of Strip 2), the EM energy from Strip 1 also fluctuates. However, because the EM energy from Strip 1 is much weaker than Strip 2 in Area B, the energy fluctuation cannot disturb the boundary conditions of Area B,. Thus, the solution in Area B remains steady, so the resonant frequency of Strip 2 stays the same.

In terms of the analysis above, benefiting from the reflection effect of the metal boundary, the resonant frequency change of one decoupling element cannot disturb the boundary conditions of the adjacent decoupling elements anymore. The stability of the boundary conditions implies steady solutions, which mean consistent resonant frequency for the decoupling elements.

D. Demonstration Example

In order to demonstrate the proposed idea, a new model with a small metal ground acting as the metal boundary between Strip 1 and Strip 2 is shown in Fig. 4(a). The newly created metal ground that only occupies 7×1 mm^2 is on the same surface of the PCB as Strip 1 and Strip 2.

From the simulated results in Fig. 4(b) and (c), it can be clearly seen that the resonant frequency of Strip 1 and Strip 2 can be tuned separately; compared to the results in Fig. 2(b), the mutual effect between Strip 1 and Strip 2 has been eliminated successfully. For further certification and comparison, in Fig. 5(a) and (b), vector current distributions are plotted for the model in Fig. 2(a). The figures show that at the resonant frequency of Strip 1 (Fig. 5(a)), there is strong energy coupled from Strip 1 to Strip 2; similarly, at the resonant frequency of Strip 2 (Fig. 5(b)), there is also strong energy coupled from Strip 2 to Strip 1; thus, the EM energy fluctuation of one strip can transmit to the other strip, which leads to the disturbance of the EM boundary conditions. In Fig. 5(c) and (d), vector current distributions are drawn for the model in Fig. 4(a). The results clearly prove that at the resonant frequency of Strip 1 (Fig. 5(c)), there is only very weak or null energy coupled from Strip 1 to Strip 2, which means that the small metal ground has blocked the energy of Strip 1 for Strip 2; at the resonant frequency of Strip 2 (Fig. 5(d)), the phenomenon is similar; hence, the EM energy fluctuation of one strip cannot transmit to the other strip anymore, so the EM boundary conditions of each strip can keep stable now. Additionally, from the vector current distributions, it can be concluded that the decoupling elements operate at 0.25λ mode like monopole antennas.

E. Discussion

Some researchers may think of other applications for the proposed idea. When an antenna element is close to a decoupling element, the decoupling element usually has large impact on the performance of the antenna element. By inserting a metal boundary, the influence of the decoupling element might be eliminated. However, the decoupling principle of

decoupling elements is to utilize the energy coupling between decoupling elements and antenna elements to create a new coupling path; the energy from the new coupling path can cancel the original coupling energy. Hence, if the decoupling elements and the antenna elements are isolated with the metal boundary, the energy coupling between them should be weakened, so the decoupling effect of the decoupling elements may become extremely weak or even disappear.

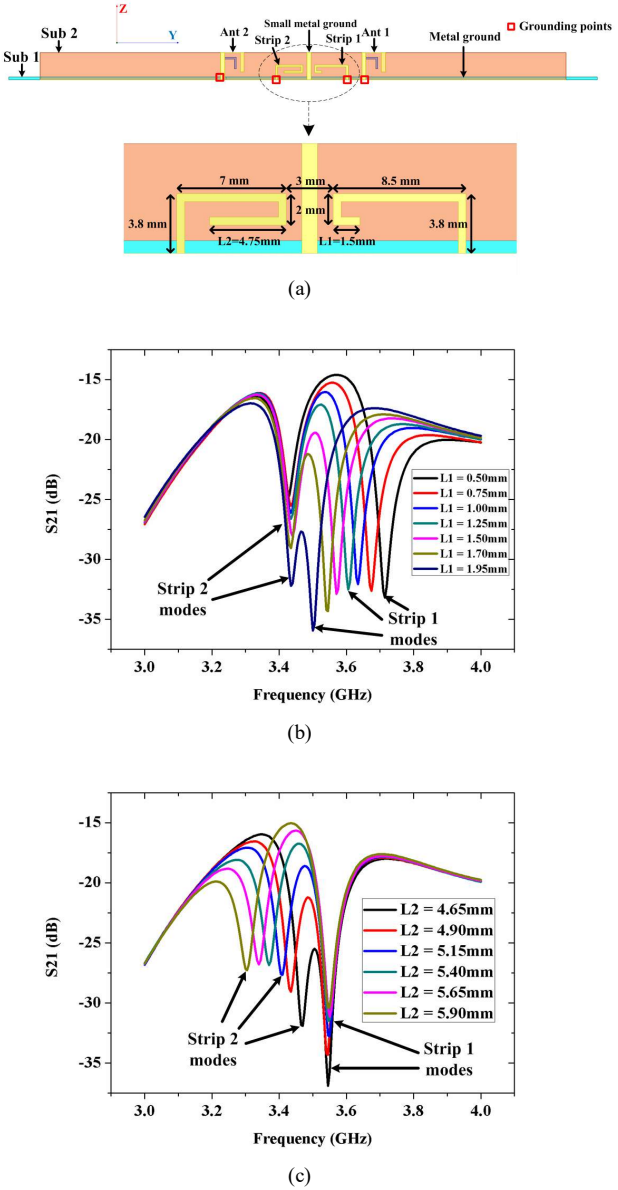

Fig. 4. Demonstration example. (a) Configuration. The resonant frequency of (b) Strip 1 and (c) Strip 2 changes.

Another possible thought is to reduce the mutual coupling between antenna elements by using the metal boundary directly. It should be emphasized that the elimination of the mutual effect between decoupling elements does not mean that there is no mutual coupling between them. The condition of weak or null mutual effect is that the energy from mutual coupling is not strong enough to disturb the EM boundary conditions of the decoupling elements. Therefore, the mutual coupling still exists. For instance, the mutual coupling between two decoupling elements is -13 dB, so only 5% energy is coupled between them. 5% energy should not be strong enough to affect the resonant frequency of the decoupling elements, but 13 dB is not a good isolation level. Thus, null mutual effect does not mean good isolation. As a result, the proposed idea can effectively eliminate the mutual effect between decoupling elements, but the metal boundary itself may not be able to reduce the mutual coupling to a very low level. The meaning of the proposed idea is to achieve multimode decoupling technique which can realize wideband/multiband high isolation.

Besides, the proposed small metal ground, which acts as the metal boundary, seems similar to the protruded metal ground in [25]. However, the protruded metal ground is actually a kind of resonant structure because there is obvious resonant feature in Fig. 9 of [25]. The decoupling elements in this paper can also be considered as a kind of slim protruded metal ground. Thus, the dimension of the protruded metal ground is relevant to its operating frequency. On the contrary, the dimension of the proposed small metal ground is independent of its operating frequency; in other words, a small metal ground with a fixed dimension can be applied to any frequency as long as its volume is big enough to block the EM energy. For instance, the same small metal ground is applied to 3.5 GHz and 2.45 GHz in Section III. As a result, the principle of the small metal ground is completely different from that of the protruded metal ground.

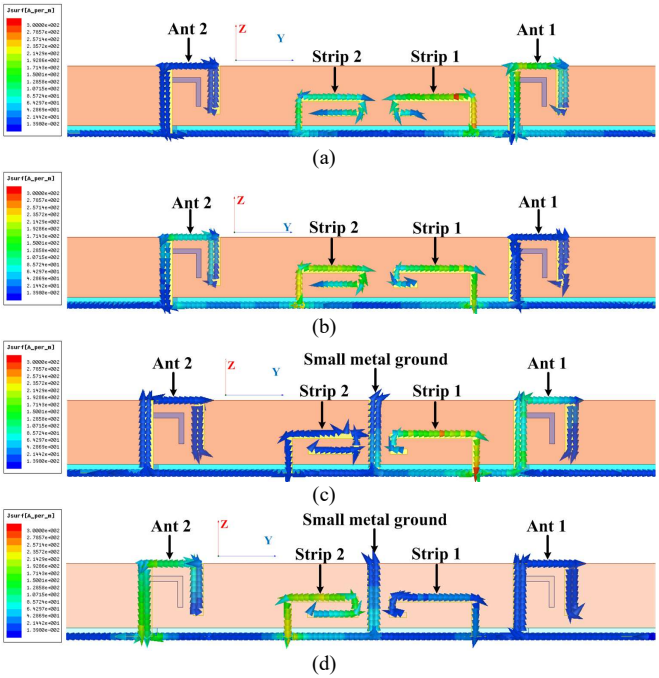

Fig. 5. Current distributions. (a) Strip 1 and (b) Strip 2 resonates without small metal ground. (c) Strip 1 and (d) Strip 2 resonates with small metal ground.

III. Multimode Decoupling Technique

By inserting N-1 metal boundaries between N decoupling elements (N = 2, 3, 4, …), multi decoupling modes can be achieved. Two case studies are shown in this section and the configuration is similar to the antenna array in Fig. 1. The detailed dimensions are shown just for Sub 2, because there are only 50 Ω microstrip lines and metal ground on Sub 1, and the

structures on Sub 3 are symmetric with that of Sub 2. Besides, the simulated and measured results are only shown for the antenna elements in Sub 2 as well. All the small metal grounds have the same dimension of 7×1 mm^2.

A. Dual-Mode Decoupling Design for A Smart Phone Side-Edge 8-Antenna Array at 3.5 GHz

The configuration is shown in Fig. 6. There are four antenna elements on Sub 2, so three dual-mode decoupling structures ($18.25\times7\times0.8$ mm^3 for each, i.e. $0.213\lambda_0\times0.082\lambda_0\times0.009\lambda_0$ at 3.5 GHz) are inserted between them. All the dual-mode decoupling structures have the same dimension in detail. In Fig. 6(b), the current maximum portion of Ant 1, Ant 2, Ant 3, and Ant 4 is on the top layer of Sub 2, while the electrical field maximum portion is on the bottom layer of Sub 2; on the edge of Sub 2, there is a 0.8 mm wide copper track connecting the two portions. The uniform width of the other antenna tracks is 1 mm, and the uniform width of the coupling lines and the decoupling elements is 0.5 mm.

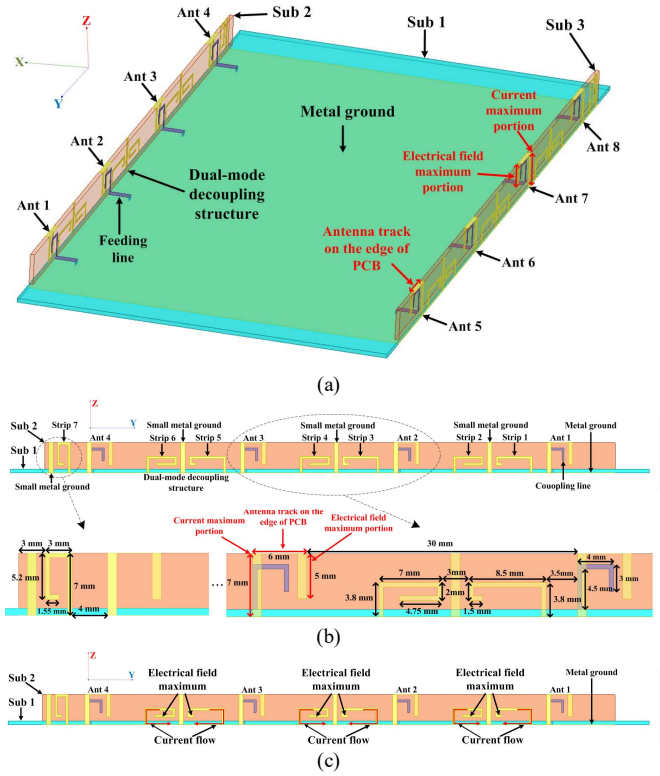

Fig. 6. Configuration of the 8-antenna array. (a) Overall view. (b) Detailed dimensions. (c) The arrangement of the energy maximum portions.

In Fig. 6(c), the consideration for the special layout can be seen clearly: the electrical field maximum portions of the decoupling elements face to the adjacent decoupling elements but not the antenna elements; although the current maximum portions are close to the antenna elements, the currents do not flow to the antenna elements because of the mirror currents on the metal ground and the current continuity theorem. In this way, the influence of the decoupling elements on the antenna elements can be minimized. The mutual effect between the decoupling elements can be eliminated with the proposed small metal ground. As a result, even if there are ten resonators in a volume of $114\times7\times0.8$ mm^3 ($1.330\lambda_0\times0.082\lambda_0\times0.009\lambda_0$ at 3.5 GHz, i.e. $0.133\lambda_0\times0.082\lambda_0\times0.009\lambda_0$ for each resonator on average), they can still operate properly.

The simulated S-parameter, antenna efficiency, and antenna pattern results are shown in Fig. 7. Comparing the results in Fig. 7(a) and (b), it can be clearly observed that the reflection coefficients are even enhanced due to the dual/multi resonance feature. According to our simulation, the resonance at around 3.58 GHz for Ant 1, Ant 2, Ant 3, and Ant 4 benefits from Strip 1, Strip 3, Strip 5, and Strip 7 respectively. Take Ant 1 and Strip 1 as an example. The current maximum portions of Strip 1 and Ant 1 are close and parallel, so Strip 1 can be coupled-fed by Ant 1 as a parasitic element. Therefore, one extra resonance is generated by Strip 1. Strip 7 is added also for the extra resonance of Ant 4.

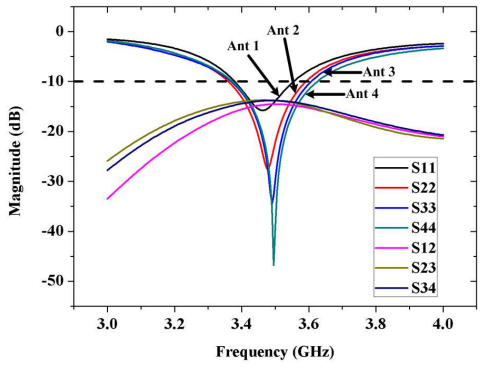

(a)

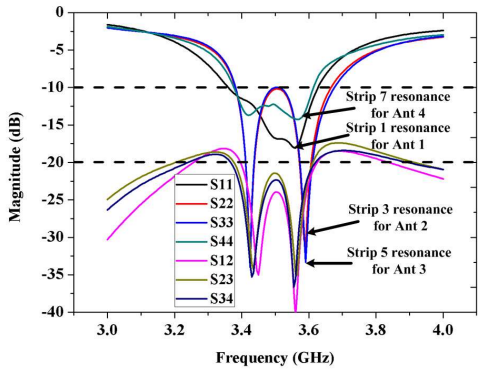

(b)

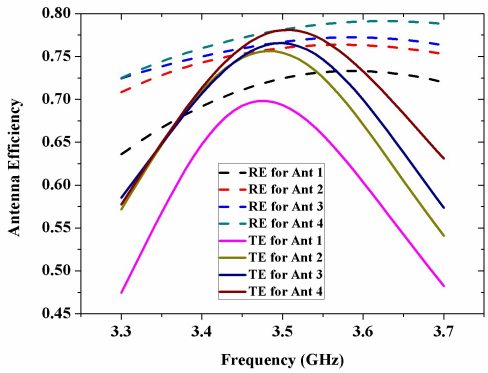

(c)

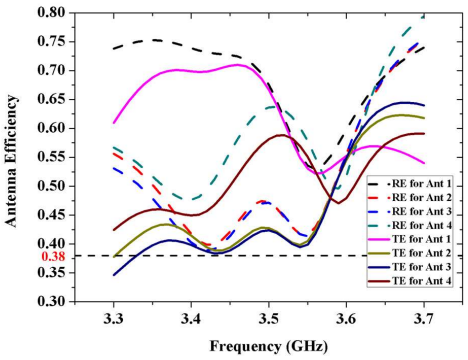

(d)

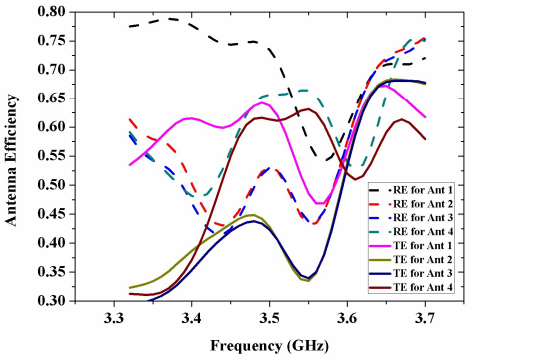

(e)

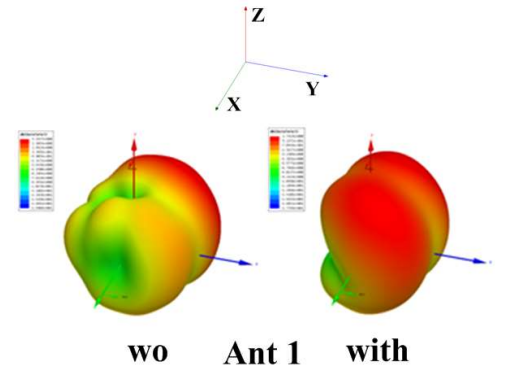

(f)

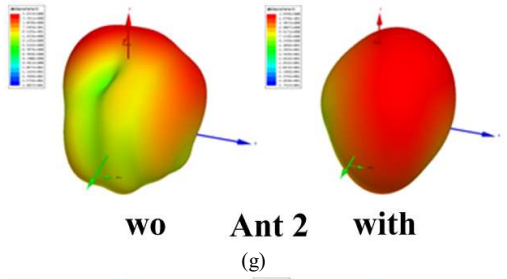

(g)

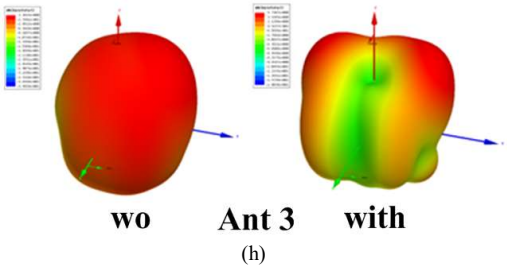

(h)

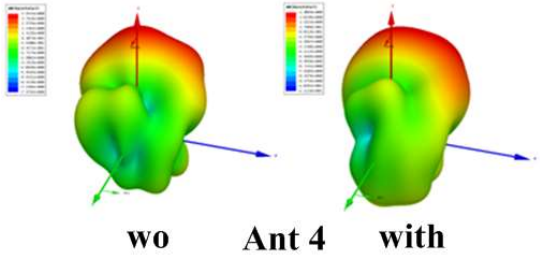

(i)

Fig. 7. Simulated results. S-parameter (a) without and (b) with decoupling elements obtained from HFSS. RE and TE (c) without and (d) with decoupling elements obtained from HFSS. (e) RE and TE with decoupling elements obtained from CST. 3D antenna patterns of (f) Ant 1, (g) Ant 2, (h) Ant 3, and (i) Ant 4 at 3.55 GHz with and without decoupling elements obtained from HFSS.

The results in Fig. 7(a) and (b) show that the isolation between Ant 1 and Ant 2, Ant 2 and Ant 3, and Ant 3 and Ant 4 is improved from 13.5 dB to > 20 dB in the frequency band of 3.4-3.6 GHz (5.7% fractional bandwidth). The isolation between Ant 1 and Ant 3, Ant 1 and Ant 4, and Ant 2 and Ant 4 is not shown because it is much better. According to our simulation, Strip 1, Strip 2, Strip 3, Strip 4, Strip 5, Strip 6, and Strip 7 can still be tuned separately. For simplicity, the results are not shown. From the results in Fig. 7(c) and (d), the decoupling structures reduce the radiation efficiency (RE) to > 39%, but the total efficiency (TE) remains > 38% within 3.4-3.6 GHz owe to the enhanced reflection coefficients. For verification of the RE and TE with decoupling elements obtained from HFSS, the results from CST is shown in Fig. 7(e). In terms of the comparison, it is evident that the results of the RE from HFSS and CST agree quite well. The results of the TE have a little bigger difference, because the simulated reflection coefficients from CST are worse than HFSS (not shown).

After adding the decoupling elements, the antenna patterns also change due to the scattering effect. According to our simulation, Strip 1, Strip 3, Strip 5, and Strip 7 have greater influence on the patterns than Strip 2, Strip 4, and Strip 6, because the radiation currents of these four decoupling elements are closer to that of the antenna elements. Thus, the 3D patterns of Ant 1, Ant 2, Ant 3, and Ant 4 with and without the decoupling elements are shown in Fig. 7(f)(g)(h)(i) at 3.55 GHz, which is the resonant frequency of Strip 1, Strip 3, Strip 5, and Strip 7. From the results, it is evident that the decoupling elements significantly affect the radiation patterns due to the small distance. Although it is not shown, the pattern variation becomes weaker and weaker as the frequency decreases.

This 8-antenna array has been fabricated and measured. The prototype and the measured S-parameter results are shown in Fig. 8(a) and Fig. 8(b) respectively. The resonant frequency of the antenna elements and the decoupling elements deviates a little due to the rough handmade prototype. The measured S12, S23, and S34 are < -20 dB in the frequency band of 3.47-3.69 GHz (6.1%), 3.42-3.66 GHz (6.8%), and 3.42-3.67 GHz (7.1%) respectively. Thus, the measured results still demonstrate the good decoupling effect of the design. In addition, this antenna array can be extended by simply duplicating the antenna elements and the decoupling elements, so it is promising for the arrays with multi antenna elements. TABLE I shows a decoupling comparison between the proposed and the reported

smart phone side-edge 8-antenna array at 3.5 GHz.

B. Quad-Mode Decoupling Design for A Smart Phone Side-Edge 4-Antenna Array at 2.45 GHz

Since there have been tri-mode decoupling designs such as [21], a quad-mode decoupling design is presented directly to show the advantage of the proposed technique. The configuration is shown in Fig. 9. There are two antenna elements on Sub 2, so one quad-mode decoupling structure (35 ×7×0.8 mm^3, i.e. 0.295λ_0×0.059λ_0×0.007λ_0 at 2.526 GHz) is inserted between them. The uniform width of the coupling lines, the antenna tracks, and the decoupling elements is 1.5 mm, 1 mm, and 0.5 mm respectively.

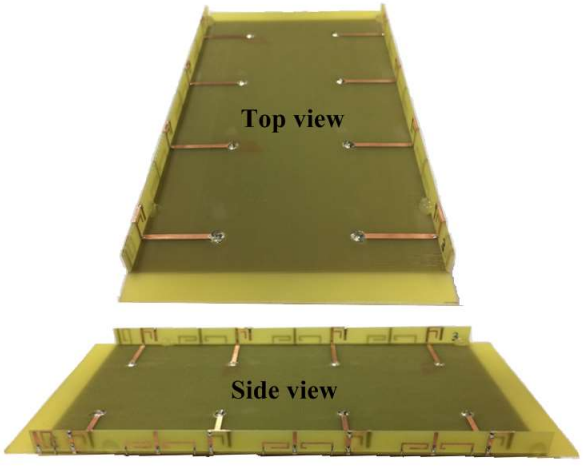

(a)

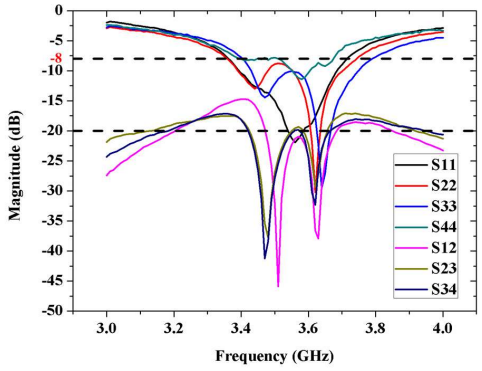

(b)

Fig. 8. (a) Fabricated prototype. (b) Measured S-parameter.

TABLE I
DECOUPLING COMPARISON

Ref. (3.5 GHz)	Proposed	[12]	[14]	[15]
Isolation (dB)	≥ 20	≥ 10	≥ 10	≥ 12
Isolation bandwidth (%)	6.1	5.7	5.7	5.7
Decoupling mode(s)	Dual-mode	None	None	Single-mode
Tuning difficulty	Easy Independent tuning	-	-	Need to design two different structures
Potential	Infinite elements in theory	-	-	Four closely-packed elements

Although the independent tuning feature has been demonstrated in Section II-D, when more decoupling elements are placed together, the mutual effect could still deteriorate because the EM coupling environment would become more complicated. According to our simulation, the mutual effect between Strip 1 and Strip 2, and Strip 3 and Strip 4 is still weak, but the mutual effect between Strip 2 and Strip 3 is relatively strong when their resonant frequency is close to each other. In order to reduce the mutual effect between Strip 2 and Strip 3, the resonant frequency of the four decoupling elements can be arranged as Strip 3, Strip 4, Strip 1, Strip 2 (the frequency increases from left to right). In this way, the resonant frequency of Strip 2 and Strip 3 is far from each other, so their mutual effect can be reduced effectively; the resonant frequency of Strip 1 and Strip 4 is close to each other, but their position is far from each other, and Strip 2 and Strip 3 can actually act as the decoupling elements between them, so the mutual effect between Strip 1 and Strip 4 is extremely weak. As a result, even if the decoupling modes are doubled, these four decoupling modes can still be tuned independently. If more decoupling elements are added, the same method can be applied.

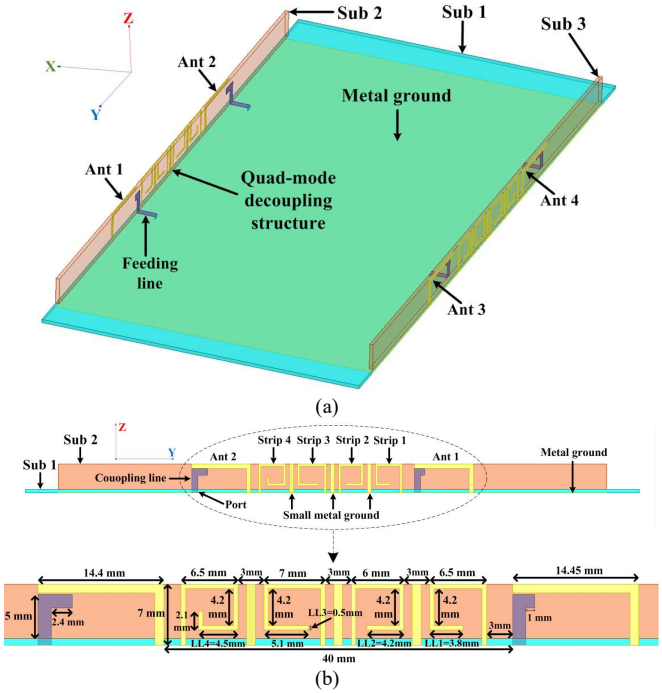

Fig. 9. Configuration of the 4-antenna array. (a) Overall view. (b) Detailed dimensions.

The simulated S-parameter, antenna efficiency, and antenna pattern results are in Fig. 10. In Fig. 10(b), the results clearly reveal that the isolation between Ant 1 and Ant 2 is improved from 12.7 dB to > 21 dB in the frequency band of 2.248-2.805 GHz (22.0% fractional bandwidth). The results in Fig. 10(c) show that the decoupling structure reduces the RE to > 43%, but the TE is still > 40% within 2.4-2.5 GHz. It can also be noticed that in the frequency band of 2.2-2.3 GHz, the TE of the Ant 2 with the decoupling elements is higher than that of the Ant 2 without the decoupling elements; this profits from the enhanced S22. For verification of the RE and TE with decoupling elements obtained from HFSS, the results from CST is shown in Fig. 10(e). According to the comparison, the results of the RE from HFSS and CST agree quite well. The results of the TE have a little bigger difference, because the

simulated reflection coefficients from CST are worse than HFSS (not shown). From the results in Fig. 10(f), (g), (h), and (i), the independent tuning characteristic of Strip 1, Strip 2, Strip 3, and Strip 4 is still good owe to the proper arrangement of their resonant frequency.

The scattering effect of the decoupling elements exists as well. In terms of the simulation, Strip 1 and Strip 2 have greater influence on the patterns of Ant 1 than Strip 3 and Strip 4 because Strip 1 and Strip 2 are closer to Ant 1; among all the decoupling elements, Strip 4 has the largest impact on Ant 2, because their radiation currents are the nearest. Therefore, the 3D patterns of Ant 1 (at 2.5 GHz which is between the resonant frequency of Strip 1 and Strip 2) and Ant 2 (at 2.4 GHz which is the resonant frequency of Strip 4) with and without the decoupling elements are shown in Fig. 10(j)(k) respectively.

This 4-antenna array has been fabricated and measured. The prototype and the measured S-parameter results are shown in Fig. 11(a) and Fig. 11(b) respectively. The resonant frequency of the antenna elements and the decoupling elements deviates a little due to the fabrication error, but the measured isolation still agrees with the simulated value well. As a result, although the bandwidth of the antenna elements is not as wide as the decoupling bandwidth, this application example still demonstrates the excellent wideband decoupling power of the proposed decoupling technique in a compact volume. Multiband decoupling can be achieved with the same method. TABLE II shows a comparison between the proposed and other reported wideband-decoupling designs in mobile terminals.

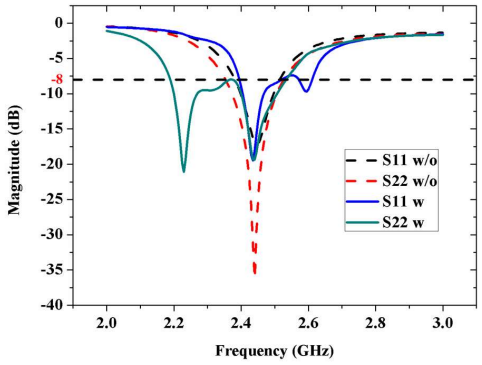

(a)

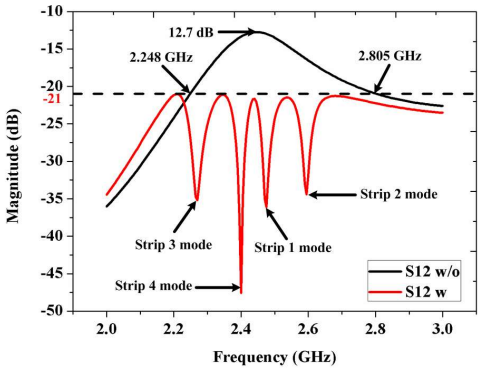

(b)

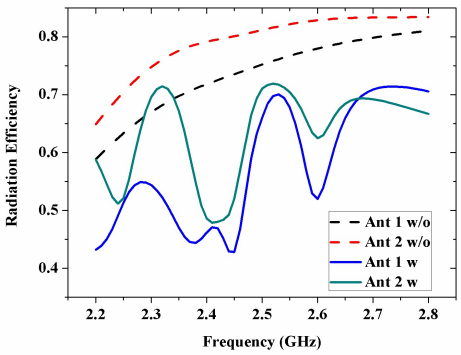

(c)

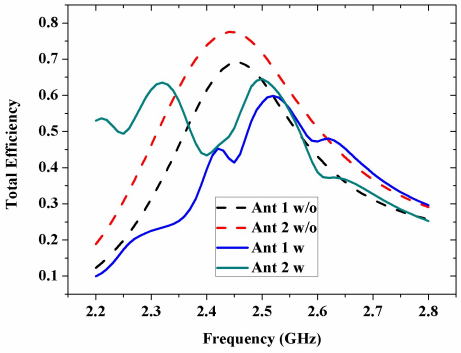

(d)

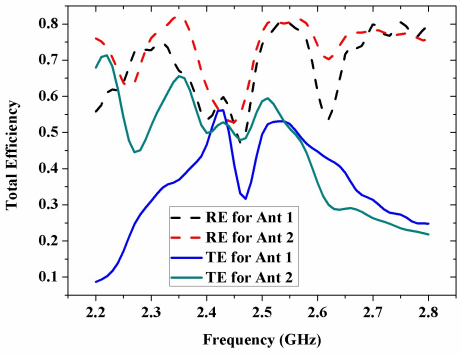

(e)

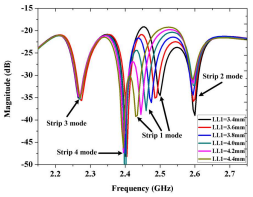

(f)

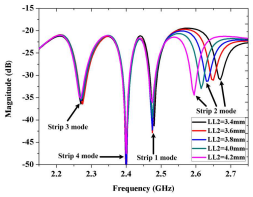

(g)

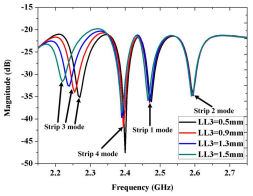

(h)

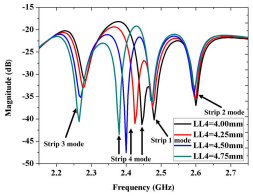

(i)

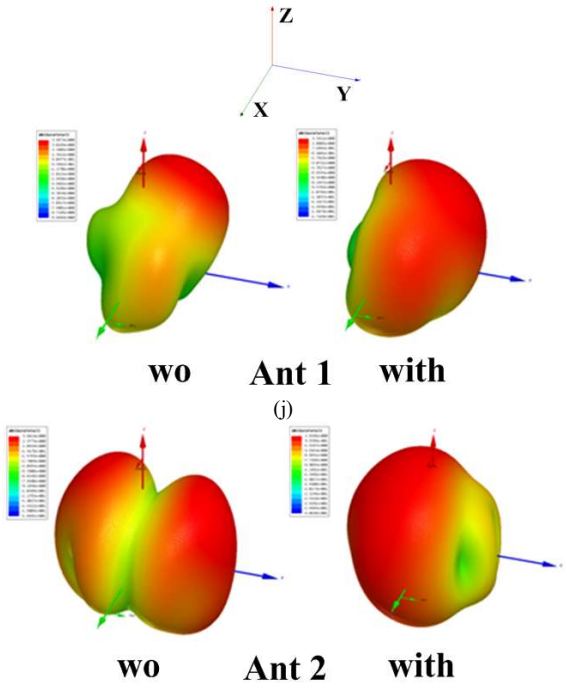

Fig. 10. Simulated results. (a) S11/S22 and (b) S12 with/without decoupling elements obtained from HFSS. (c) RE and (d) TE with/without decoupling elements from HFSS. (e) RE and TE with decoupling elements from CST. Resonant frequency of (f) Strip 1, (g) Strip 2, (h) Strip 3, and (i) Strip 4 changes obtained from HFSS. 3D antenna patterns of (j) Ant 1 at 2.5 GHz and (k) Ant 2 at 2.4 GHz with and without decoupling elements obtained from HFSS.

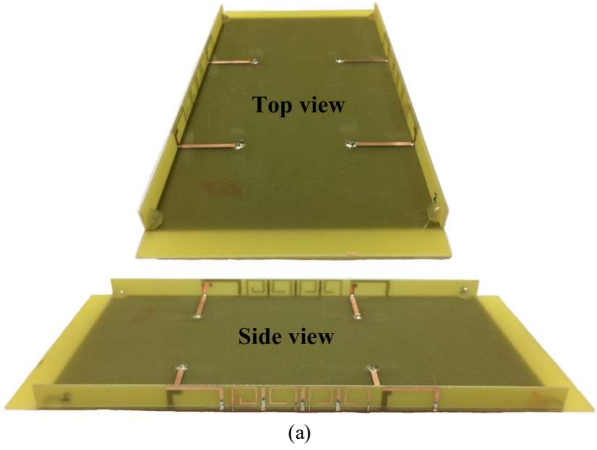

Fig. 11. (a) Fabricated prototype. (b) Measured S-parameter.

C. *The Impact of Smart Phone Components*

The impact of some smart phone components at different distance from the antenna arrays is researched. All the components are imitated by using metal blocks. When a battery ($70\times40\times3$ mm^3) is placed in the middle of the smart phone, the performance has little degradation except 4% reduction of the total efficiency, so the results are not shown for simplicity.

In Fig. 12(a), a USB connector ($10\times8\times3$ mm^3) and a metal housing (120 mm$\times$(75 mm-*DD*1/*DD*2)$\times$3 mm) are put on the top of Sub 1 for each antenna array. One rectangular block is removed from the whole metal housing for each feeding port to ensure normal excitation. The simulated S-parameter and total efficiency are presented in Fig. 12(b)(c)(d). There are loads of data, so only some typical antenna elements were adopted for analysis and explanation.

For the 8-antenna array, the performance change of Ant 2 is shown. At *DD*1 = 3, 4, 5 mm, the reflection coefficient of Ant 2 has little deterioration, but the total efficiency decreases to 30% due to the absorption effect of the metal housing. At *DD*1 = 2 mm, the resonant frequency of Ant 2 decreases obviously, because the metal housing is close to the open-end of the antenna and thus provide a capacitive-loading. At *DD*1 = 1 mm, the performance of the antenna has been destroyed. At all the parameters, the isolation between Ant 2 and Ant 3 keeps a good level of > 19 dB within 3.4-3.6 GHz. The phenomena are similar in other antenna elements.

The situation is better in the 4-antenna array, because the open-end of the antenna elements is somewhat far from the metal housing so the capacitive-loading effect is relatively weak. Ant 1 was adopted as the example. At *DD*2 = 3, 4, 5 mm, there is little degradation in the reflection coefficient, but the isolation between Ant 1 and Ant 2 declines to 16 dB at *DD*2 = 5 mm due to the resonant frequency variation of the decoupling elements. At *DD*2 = 1, 2 mm, the resonant frequency of Ant 1 actually increases rather than decreases, so the frequency point of the worst S21 rises as well. The peak point of the total efficiency varies along with the resonant frequency of Ant 1. The phenomena are similar in other antenna elements.

D. *User's Hand Effects*

The effect of a user's hand(s) on the antenna performance is investigated including single-hand operation (SHO) and dual-hand operation (DHO), which are depicted in Fig. 13(a). The antenna arrays at 2.45 GHz and 3.5 GHz normally operate at data mode, so the effect of a user's head is not considered.

For SHO mode, the simulated S-parameter and total efficiency are shown in Fig. 13(b)(c). For the 8-antenna array, Ant 2, Ant 5, and Ant 6 are directly contacted by the hand, so their performance has the largest degradation: the reflection coefficients are influenced dramatically, and the efficiency declined to < 10% due to the absorption effect of the hand. Ant 1 is not contacted but very close to the hand, so its efficiency is lower than the other four antenna elements. The isolation between Ant 3 and Ant 4, and Ant 7 and Ant 8 remains consistent, but the isolation between other antenna elements actually becomes much better, because much EM energy has been absorbed. The phenomena are similar in the 4-antenna

array. The performance of Ant 1 and Ant 3 deteriorates the most because of the direct contact of the hand, and the isolation between antenna elements increases to > 30 dB owe to the absorption of the EM energy.

For DHO mode, the situation is better, because the hands do not contact the antenna elements directly. The simulated S-parameter and total efficiency are shown in Fig. 13(d)(e). For the 8-antenna array, the reflection coefficients have little deterioration, but the resonant frequency of the decoupling elements varies a little. However, the isolation is still > 18 dB within the operating frequency band. The efficiency decreases due to the absorption effect of the hands. The change is analogous in the 4-antenna array. The S-parameter has minute degradation and the efficiency declines.

IV. Conclusion

The essence of the strong mutual effect between closely-packed decoupling elements has been explained from the perspective of mathematical physics. A novel idea of achieving the stability of the boundary conditions of decoupling elements has been proposed and solved the mutual effect problem simply and effectively; in physical structure, a metal boundary has been adopted to realize the stability.

By isolating multi decoupling elements, multimode decoupling technique has been achieved for mobile terminals. The proposed technique can accomplish wideband/multiband high isolation and easy tuning feature in a compact volume.

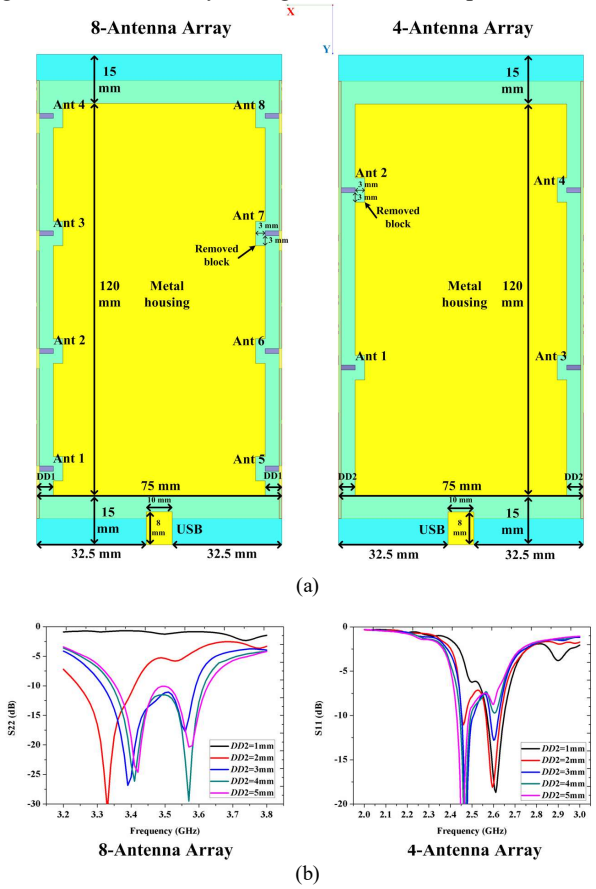

(a)

(b)

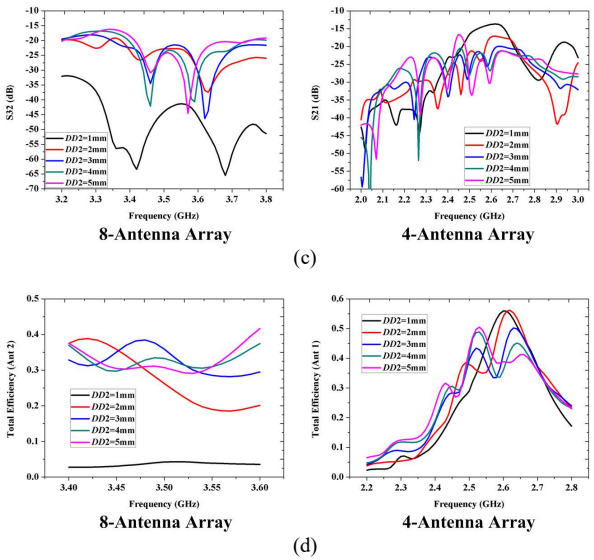

(c)

(d)

Fig. 12. The impact of a metal housing and a USB connector. (a) Simulation models. (b) Reflection coefficients, (c) mutual coupling, and (d) total efficiency of Ant 2 in the 8-antenna array and Ant 1 in the 4-antenna array.

TABLE II
WIDEBAND-DECOUPLING COMPARISON

Ref.	Enhanced isolation	Enhanced bandwidth	Volume (λ_0^3)	Design difficulty	Processing technology
[18]	13 dB	11%	0.026× 0.020× 0.010	Not easy	LTCC
[21]	7 dB	20.1%	0.390× 0.050× 0.006	Not easy	PCB
[22]	7 dB	109%	0.622× 0.183× 0.018	Not shown	PCB
This paper	8.3 dB	22%	0.295× 0.059× 0.007	Easy tuning	PCB

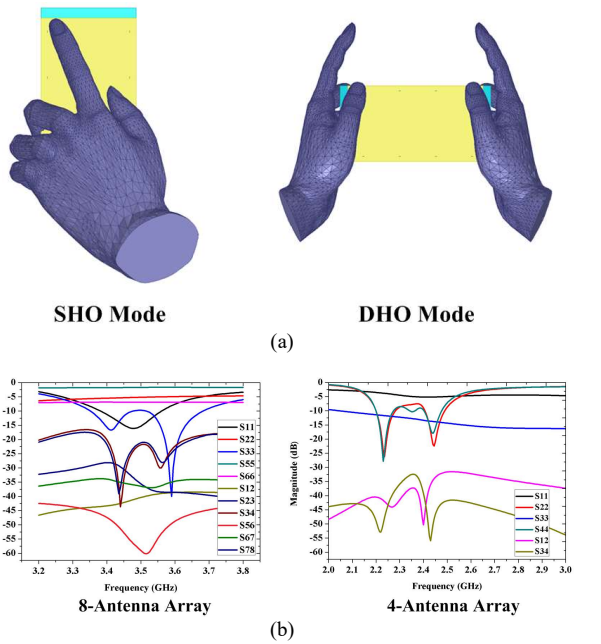

(a)

(b)

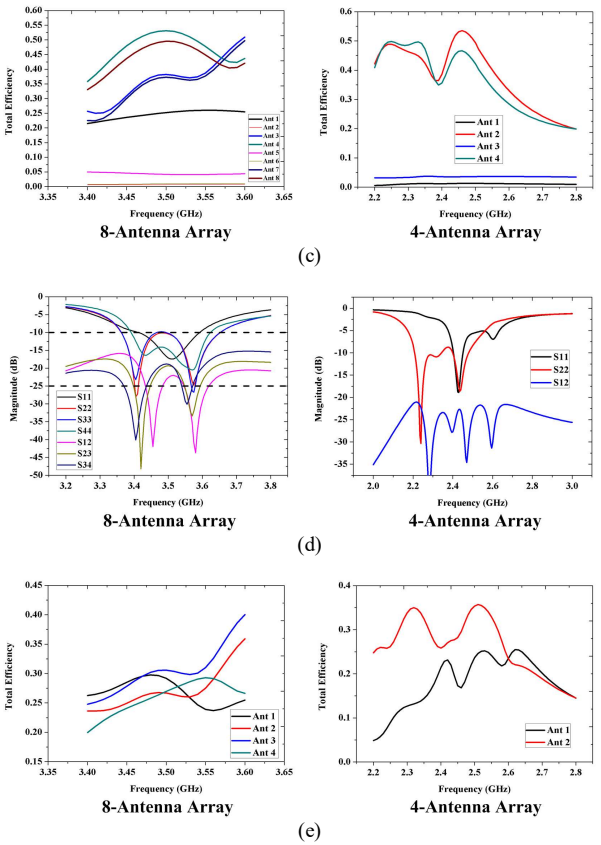

Fig. 13. The effect of a user's hand(s). (a) Two typical usage scenarios. (b) S-parameter and (c) total efficiency of the 8-antenna array and 4-antenna array at SHO mode. (d) S-parameter and (e) total efficiency of the 8-antenna array and 4-antenna array at DHO mode. All the results were obtained from HFSS.

REFERENCES

[1] J.G. Andrews, et al, "What Will 5G Be?," *IEEE J. Sel. Areas Commun,* vol. 32, no. 6, pp. 1065-1082, Jun. 2014.

[2] S.M. Razavizadeh, et al, "Three-Dimensional Beamforming: A new enabling technology for 5G wireless networks," *IEEE Signal Processing Mag.*, vol. 31, no. 6, pp. 94–101, Nov. 2014.

[3] A. Sabharwal, et al, "In-Band Full-Duplex Wireless: Challenges and Opportunities," *IEEE J. Sel. Areas Commun,* vol. 32, no. 9, pp. 1637-1652, Sep. 2014.

[4] Q. Luo, S. Gao, et al, "Design and Analysis of a Reflectarray Using Slot Antenna Elements for Ka-band SatCom," *IEEE Trans. Antennas Propag.*, vol. 63, no. 4, pp. 1365–1374, Apr. 2015.

[5] X. Ding, et al, "A Wide-Angle Scanning Planar Phased Array with Pattern Reconfigurable Magnetic Current Element," *IEEE Trans. Antennas Propag.*, vol. 65, no. 3, pp. 1434–1439, Mar. 2017.

[6] C.-Y. Chiu, C.-H. Cheng, R. D. Murch, and C. R. Rowell, "Reduction of mutual coupling between closely-packed antenna elements," *IEEE Trans. Antennas Propag.*, vol. 55, no. 6, pp. 1732–1738, Jun. 2007.

[7] S. Gao, et al, "A Broad-Band Dual-polarized Microstrip Patch Antenna with Aperture Coupling," *IEEE Trans. Antennas Propag.*, vol. 51, no. 4, pp. 898–900, Apr. 2003.

[8] H. Li, et al, "Design of Orthogonal MIMO Handset Antennas Based on Characteristic Mode Manipulation at Frequency Bands Below 1 GHz," *IEEE Trans. Antennas Propag.*, vol. 62, no. 5, pp. 2756–2766, May. 2014.

[9] S.-C. Chen, et al, "A decoupling technique for increasing the port isolation between two strongly coupled antennas," *IEEE Trans. Antennas Propag.*, vol. 56, no. 12, pp. 3650–3658, Dec. 2008.

[10] A. Diallo, et al, "Study and reduction of the mutual coupling between two mobile phone PIFAs operating in the DCS 1800 and UMTS bands," *IEEE Trans. Antennas Propag.*, vol. 54, no. 11, pp. 3063–3074, Nov. 2006.

[11] A.C. K.Mak, C. R. Rowell, and R.D. Murch, "Isolation enhancement between two closely packed antennas," *IEEE Trans. Antennas Propag.*, vol. 56, no. 11, pp. 3411–3419, Nov. 2008.

[12] A. A. Al-Hadi, et al, "Eight-element antenna array for diversity and mimo mobile terminal in LTE 3500 MHz band," *Microw. Opt. Technol. Lett.*, vol. 56, no. 6, pp. 1323-1327, Jun. 2014.

[13] K.L. Wong and J.Y. Lu, "3.6-GHz 10-ANTENNA ARRAY FOR MIMO OPERATION IN THE SMARTPHONE," *Microw. Opt. Technol. Lett.*, vol. 57, no. 7, pp. 16991704, Jul. 2015.

[14] Y.L. Ban, et al, "4G/5G Multiple Antennas for Future Multi-Mode Smartphone Applications," *IEEE Access*, vol. 4, pp. 2981-2988, 2016.

[15] K.L. Wong, et al, "8-Antenna and 16-Antenna Arrays Using The Quad-Antenna Linear Array as A Building Block for The 3.5-GHz LTE MIMO Operation in The Smartphone," *Microw. Opt. Technol. Lett.*, vol. 58, no. 1, pp. 174-181, Jan. 2016.

[16] M.Y. Li, Y.L. Ban, et al, "Eight-Port Orthogonally Dual-Polarized Antenna Array for 5G Smartphone Applications," *IEEE Trans. Antennas Propag.*, vol. 64, no. 9, pp. 3820–3830, Jun. 2016.

[17] L.Y. Zhao and K.L. Wu, "A Dual-Band Coupled Resonator Decoupling Network for Two Coupled Antennas," *IEEE Trans. Antennas Propag.*, vol. 63, no. 7, pp. 2843–2850, Jul. 2015.

[18] K.W. Qian, L.Y. Zhao, and K.L. Wu, "An LTCC Coupled Resonator Decoupling Network for Two Antennas," *IEEE Trans. Microw. Theory Techn.*, vol. 63, no. 10, pp. 3199–3207 Oct. 2015.

[19] L.Y. Zhao, et al, "A Coupled Resonator Decoupling Network for Two-Element Compact Antenna Arrays in Mobile Terminals," *IEEE Trans. Antennas Propag.*, vol. 62, no. 5, pp. 2767–2776, May 2014.

[20] L.Y. Zhao, et al, "A Cascaded Coupled Resonator Decoupling Network for Mitigating Interference Between Two Radios in Adjacent Frequency Bands," *IEEE Trans. Microw. Theory Techn.*, vol. 62, no. 11, pp. 2680–2688, Nov. 2014.

[21] Y. Wang and Z.W. Du, "A Wideband Printed Dual-Antenna With Three Neutralization Lines for Mobile Terminals," *IEEE Trans. Antennas Propag.*, vol. 62, no. 3, pp. 1495–1500, Mar. 2014.

[22] S. Zhang, Z. Ying, J. Xiong, and S. He, "Ultrawideband MIMO/Diversity Antennas with a Tree-Like Structure to Enhance Wideband Isolation," *IEEE Antennas Wireless Propag. Lett.*, vol. 8, pp.1279-1282, 2009.

[23] H. Li, J. Xiong, Z. Ying and S. He, "Compact and Low Profile Co-located MIMO Antenna Structure with Polarization Diversity and High Port Isolation," *Electronic Letters*, vol. 46, no. 2, pp.108-110, Jan. 2010.

[24] J.M. Jin, *Theory and Computation of Electromagnetic Fields*, John Wiley & Sons, 2010, ch. 1-3.

[25] Y.L. Ban, et al, "Decoupled Closely Spaced Heptaband Antenna Array for WWAN/LTE Smartphone Applications," *IEEE Antennas Wireless Propag. Lett.*, vol. 13, pp. 31-34, 2014.

Hang Xu received his B.S. and M.S. degrees from the University of Electronic Science and Technology of China, Chengdu, China, in 2009 and 2013 respectively. He is currently pursuing the Ph.D. degree at University of Kent, Canterbury, United Kingdom.

His research interests include 5G smartphone antennas, MIMO antenna arrays, decoupling technology, microwave and millimeter-wave antennas.

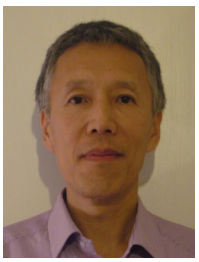

Hai Zhou received a Ph.D. degree on reflector antenna synthesis in 1987 from University of London, where he also carried out his post doctoral work until 1992.

He served as a senior lecturer at South Bank University, London before joining Lucent Technologies in 1996, working on GSM, UMTS and LTE in system engineering before joining Huawei Technologies in 2015. He worked on various topics from shaped reflector antenna synthesis, FDTD during his academic years to radio resource management and adaptive antennas in industry, with 18 patents, 14 journal papers and 34 conference papers. One of the papers won the Best Paper Award at the 19th European Microwave Conference in 1989, another received Oliver Lodge premium from IEE as the best paper of the year on Antennas and Propagation in 1991.

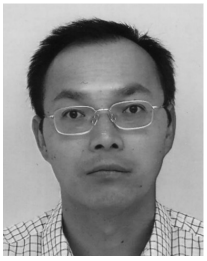

Steven Gao (M'01–SM'16) received the Ph.D. degree in Microwave Engineering from Shanghai University, Shanghai, China.

He is a Professor and Chair of RF and Microwave Engineering with the University of Kent, Canterbury, U.K. He started his career since 1994 while at China Research Institute of Radiowave Propagation. Afterward, he worked as a Post-doctoral Research Fellow with the National University of Singapore, Singapore, a Research Fellow with Birmingham University, Birmingham, U.K., a Visiting Research Scientist at Swiss Federal Institute of Technology (ETHZ), Zürich, Switzerland, a Visiting Fellow at Chiba University (Japan), a Visiting Scientist at the University of California at Santa Barbara, Santa Barbara, USA, a Senior Lecturer, Reader, and Head of Antenna and Microwave Group with Northumbria University, Newcastle upon Tyne, U.K., and the Head of Satellite Antennas and RF System Group with Surrey Space Centre, University of Surrey, Surrey, U.K. He is a Professor with the University of Kent, since January 2013. He is an IEEE AP-S Distinguished Lecturer, an Associate Editor of IEEE Trans. on Antennas and Propagation, an Associate Editor of Radio Science, and Editor-in-Chief for Wiley Book Series on "Microwave and Wireless Technologies." He co-edited Space Antenna Handbook (Wiley, 2012) and co-authored Circularly Polarized Antennas (IEEE-Wiley, 2014), over 250 papers and several patents. His research interests include smart antennas, phased arrays, MIMO, satellite antennas, microwave/mm-wave/THz circuits, satellite and mobile communications, and radar (UWB radar, synthetic-aperture radar) and wireless power transfer.

Dr. Gao is a Fellow of IET, U.K, was General Chair of LAPC 2013, and an Invited or Keynote Speaker of some international conferences such as AES'2014, IWAT'2014, SOMIRES'2013, and APCAP'2014 .

Hanyang Wang (SM'03) received the Ph.D. degree from Heriot-Watt University, Edinburgh, U.K., in 1995.

He was a Lecturer and an Associate Professor with Shandong University, Jinan, China, from 1986 to 1991. From 1995 to 1999, he was a Post-Doctoral Research Fellow with the University of Birmingham, Birmingham, U.K., and the University of Essex, Colchester, U.K. From 1999 to 2000, he was with Vector Fields Ltd., Oxford, U.K., as a Software Development and Microwave Engineering Consultant Engineer. He joined Nokia U.K. Ltd., Farnborough, U.K., in 2001, where he was a Mobile Antenna Specialist for 11 years. He then joined Huawei Technologies, where he is currently the Chief Mobile Antenna Expert and the Head of the Mobile Antenna Technology Division. He is also an Adjunct Professor with the School of Electronics and Information Technology, Sichuan University, Chengdu, China. He holds over 40 granted and pending US/WO/PCT patents, and he has authored over 80 refereed papers on these topics. His current research interests include small antennas for mobile terminals, patch and slotted waveguide antennas and arrays for mobile communications and airborne radars, and numerical methods for the solutions of electromagnetic radiation and scattering problems.

Dr. Wang is a Huawei Fellow and an IET/IEE Fellow. He was a recipient of the Title of Nokia Inventor of the Year in 2005, the Nokia Excellence Award in 2011, the Huawei Individual Gold Medal Award in 2012, and the Huawei Team Gold Medal Award in 2013 and 2014, respectively. His patent was ranked number one among the 2015 Huawei top ten patent awards. He is an Associate Editor of the IEEE Antennas and Wireless Propagation Letters. He is listed in Marquis *Who's Who in the World* and the International Biographical Center, Cambridge, U.K.

Yujian Cheng (SM'14) was born in Sichuan Province, China, on April, 1983. He received the B. S. degree from University of Electronic Science and Technology of China, in 2005 and the Ph.D. degree without going through the conventional Master's degree at Southeast University, Nanjing, China, in 2010.

Since 2010, he has been with the School of Electric Engineering, University of Electronic Science and Technology of China, and is currently a Professor. From 2012 to 2013, he was a research staff in the Department of Electrical and Computer Engineering, National University of Singapore. His current research interests include microwave and millimeter-wave antennas, arrays and circuits. He has authored or coauthored more than 100 papers in journals and conferences, as well as a book-Substrate Integrated Antennas and Arrays, (CRC press, 2015).

Dr. Cheng was the recipient of the National Science Fund for Excellent Young Scholars in 2016, Chang Jiang Scholars Program (Young Scholars) in 2016, the National Program for Support of Top-Notch Young Professionals in 2014, New Century Excellent Talents in University in 2013, and National Excellent Doctorate Dissertation of China in 2012. He is currently the secretary of the joint IEEE Chapters of APS/EMCS, Chengdu, China. He is the Senior Member of the Chinese Institute of Electronics. Now, Cheng has served as the Associate Editor for IEEE Antennas and Wireless Propagation Letters, and on review boards of various technical journals.